

# THREE-DIMENSIONAL ANALYSIS OF REINFORCED CONCRETE BEAM-COLUMN STRUCTURES IN FIRE

by Zhaohui Huang<sup>1</sup>, Ian W. Burgess<sup>2</sup> and Roger J. Plank<sup>3</sup>

## ABSTRACT

In this paper a robust non-linear finite element procedure is developed for three-dimensional modelling of reinforced concrete beam-column structures in fire conditions. Because of the changes in material properties and the large deflections experienced in fire, both geometric and material non-linearities are taken into account in this formulation. The cross-section of the beam-column is divided into a matrix of segments, and each segment may have different material, temperature and mechanical properties. The more complicated aspects of structural behaviour in fire conditions, such as thermal expansion, transient state strains in the concrete, cracking or crushing of concrete, yielding of steel and change of material properties with temperature are modelled. A void segment is developed to effectively model the effect of concrete spalling on the fire resistance of concrete beam-column members. The model developed can be used to quantify the residual strength of spalled reinforced concrete beam-column structures in fire. A series of comprehensive validations have been conducted to validate the model. From this research it can be concluded that the influence of transient state strains of concrete on the deflection of structures can be very significant. However, there is very little effect on the failure time of a simple structural member. The impact of concrete spalling on both the thermal and structural behaviour of reinforced concrete members is very significant. It is vitally important to consider the prospect of concrete spalling in fire safety design for reinforced concrete buildings.

**Key words:** concrete spalling; geometrical non-linearity; beam-column element; segmentation; fire resistance, reinforced concrete structures.

<sup>1</sup> Lecturer, Member, ASCE, Department of Civil and Structural Engineering, The University of Sheffield, Sheffield, S1 3JD, UK. Tel: +44-(0)114-2225710, Fax: +44-(0)114-2225700, Email:

[z.huang@sheffield.ac.uk](mailto:z.huang@sheffield.ac.uk)

<sup>2</sup> Professor, Department of Civil and Structural Engineering, The University of Sheffield, Sheffield, S1 3JD, UK. Email: [ian.burgess@sheffield.ac.uk](mailto:ian.burgess@sheffield.ac.uk)

<sup>3</sup> Professor, School of Architectural Studies, The University of Sheffield, Sheffield, S10 2TN, UK. Email: [r.j.plank@sheffield.ac.uk](mailto:r.j.plank@sheffield.ac.uk)

## Notation

The following symbols are used in this paper:

$a_k, b_k$	cross-sectional dimensions of the beam at nodal point $k$
${}^t_0 \mathbf{B}_L$	linear strain-displacement transformation matrix in global coordinates
${}^t_0 \overline{\mathbf{B}}_{NL}$	non-linear strain-displacement transformation matrix in local coordinates
${}^t_0 \mathbf{B}_{NL}$	non-linear strain-displacement transformation matrix in global coordinates
$\mathbf{D}'$	material constitutive matrix
$E_t$	tangent modulus of the material
$G$	shear modulus
${}^t_0 \mathbf{F}$	element internal force vector
$\mathbf{K}_T$	element stiffness matrix
${}^t_0 \overline{\mathbf{S}}$	Piola-Kirchhoff stress vector
$t'$	(superscript) indicates at time $t'$
$r, s, t$	natural coordinates
$\Delta t^k, \Delta s^k$	offsets of reference axis from the central of the cross-section at nodal point $k$ in $t$ and $s$ directions
${}^t V_{tx}^k, {}^t V_{ty}^k, {}^t V_{tz}^k$	components of unit vector ${}^t \mathbf{V}_t^k$ in direction $t$ at nodal point $k$
${}^t V_{sx}^k, {}^t V_{sy}^k, {}^t V_{sz}^k$	components of unit vector ${}^t \mathbf{V}_s^k$ in direction $s$ at nodal point $k$
$x, y, z$	global Cartesian coordinates
$x', y', z'$	local coordinates
${}^t x, {}^t y, {}^t z$	global Cartesian coordinates of any point in the element at time $t'$
${}^t x^k, {}^t y^k, {}^t z^k$	global Cartesian coordinates of nodal point $k$ at time $t'$
${}^t \boldsymbol{\varepsilon}_T$	total thermal strain vector
${}^t \boldsymbol{\varepsilon}_{tr}$	total transient state strain vector of concrete (for reinforcing steel segments ${}^t \boldsymbol{\varepsilon}_{tr} = \mathbf{0}$ )
${}^t_0 \boldsymbol{\varepsilon}$	Green-Lagrange strain vector
$\Delta \boldsymbol{\varepsilon}$	strain increment vector in local coordinates
$0$	(superscript or subscript) indicates relative to initial configuration

## INTRODUCTION

The behaviour of structures exposed to fire is usually described in terms of the concept of fire resistance, which is the period of time under exposure to a standard fire time-temperature curve at which some prescribed form of limiting behaviour occurs. In performance-based design this limiting behaviour may be defined either as real structural collapse or as a failure of integrity which would allow fire-spread to occur, but is more usually defined in terms of a deflection limit. The most recent design codes, EN 1992-1-2 (2004) and EN 1994-1-2 (2005) have taken a step towards full performance-based design by allowing designers to treat fire as one of the basic design limit states, taking account of:

- Non-uniform heating due to partial protection, which may be inherent in the framing system or specially applied,
- The level of loading at the fire limit state, using partial safety factors lower than those used for ultimate limit states, because of the relative improbability of such accidental combinations,
- Realistic stress-strain characteristics of structural materials at elevated temperatures.

The main limitation of these codified approaches is that they are based on the behaviour under test of isolated simply supported members, usually heated according to the standard ISO834 (1985) time-temperature curve. In real buildings structural elements form part of a continuous assembly, and building fires often remain localised, with the fire-affected region of the structure being subject to significant restraint from cooler areas surrounding it. The real behaviour of these structural elements can therefore be very different from that indicated by standard furnace tests.

The six large fire tests carried out in 1995-96 on a full-scale composite building at the BRE Fire Research Laboratory at Cardington (Swinden Technology Centre 1999) made it clear that unprotected steel members could have significantly greater fire resistance as part of real multi-storey buildings than when tested as isolated members. This is undoubtedly due to interaction between the heated members within the fire compartment, the concrete floor slabs (both heated and unheated) and the adjacent composite frame structure. If such interactions are to be used by designers in specifying fire protection strategies as part of an integrated limit state structural design process rather than as an adjunct to it, then this can not practically be based on large-scale testing because of the extremely high implicit costs. It is therefore becoming increasingly important that software models be developed to enable the behaviour of such structures to be predicted with sufficient accuracy under fire conditions.

In recent years a number of numerical models have been developed to represent the behaviour of reinforced concrete structures in fire (Ellingwood and Lin 1991; Huang and Platten 1997; Terro 1998; Capua and Mari 2007; Bratina et al. 2007), but none of these have taken the phenomenon of spalling into account. Due to its complexity, current design codes, such as EN 1992-1-2 (2004) provide only simple guidance on the influence of spalling on the fire resistance of concrete structures. At present there is no robust method available to assess the residual strength of a structure after spalling has occurred to some members. It is therefore very important that a comprehensive procedure be developed which can assess the impact on global structural behaviour of the occurrence of spalling to certain reinforced concrete members.

The specialised finite element program *Vulcan* has been progressively developed over the past decade (Najjar and Burgess 1996; Bailey *et al.* 1996; Huang *et al.* 1999a; Huang *et al.* 2003a; Cai *et al.* 2002) at the University of Sheffield for three-dimensional modelling of the structural behaviour of composite and steel-framed buildings in fire. As part of this program a non-linear layered finite element procedure has been developed for predicting the structural response of reinforced concrete slabs subjected to fire (Huang *et al.* 2003a). The procedure is based on Mindlin/Reissner (thick plate) theory, and both geometric and material non-linearities are taken into account. The complexities of structural behaviour in fire conditions, caused by thermal expansion, cracking or crushing, and change of material properties with temperature, are modelled.

In the original formulation beams and columns were represented by two-noded one-dimensional line elements in which each node had 8 degrees of freedom in local coordinates, which were transformed to 11 apparent degrees of freedom in global coordinates (Najjar and Burgess 1996; Cai *et al.* 2002). Apart from the normal three translational and three rotational degrees of freedom, five extra degrees of freedom existed, representing three derivatives of displacement (“strains”), plus twisting and warping degrees of freedom. Although these elements proved extremely accurate up to, and beyond, the deflection levels which are practically acceptable in building structures in fire conditions, there were some major disadvantages to using this approach:

- Because of the five unconventional degrees of freedom at each node the processing time was high compared to analyses using the normal six degrees of freedom;
- It was always necessary to apply internal constraints to some of the nodal degrees of freedom, even when no external boundary constraints existed;
- There were some logical difficulties in setting nodal constraint conditions for members not parallel to the global coordinate axes. Different specification of these constraints for such

members could influence the results of analyses quite significantly, especially when displacements were large (Wong 2001).

Because of these aspects a re-formulation has been undertaken, with the primary objective of developing a more robust non-linear beam-column element for three-dimensional modelling of reinforced concrete frame members in fire conditions in which the effects of spalled concrete on both thermal and structural behaviour could easily be taken into account.

## **NON-LINEAR PROCEDURE**

From finite element literature it is evident that a large number of beam element formulations have been proposed for general non-linear analysis (Bathe and Bolourchi 1979; Surana and Sorem 1989). Beam elements based on an isoparametric formulation are particularly attractive because of the consistent formulation that is used, their generality in use and their computational efficiency. In this work a general three-dimensional isoparametric 3-noded beam-column element has been developed for modelling of beam-columns of composite steel-concrete or reinforced concrete cross-sections in elevated-temperature conditions. The proposed model is based on a formulation proposed by Bathe (1982) for geometrically non-linear modelling of elastic beams. The non-linear procedure developed in this paper takes into account both geometric and material non-linearities and the effects of spalled concrete. In order to allow for different thermal distributions across members, and the thermal strains and changes of material properties which accompany these temperatures, the cross-section of the beam-column element is divided into a matrix of segments; each segment can then have different material, thermal and mechanical properties. The more complex aspects of concrete structural behaviour in fire conditions, such as thermal expansion, transient state strain, degradation of stress-strain curves, failure of concrete segments by cracking and crushing, and yielding of steel profile or reinforcement segments, are included.

Using the general continuum mechanics equations for large-displacement non-linear analysis, the calculation of the non-linear beam element matrices represents a direct extension of the linear (small displacement) formulation. The calculations are performed, as in the evaluation of the matrices of the elements, using the conventional six “displacement” degrees of freedom only. The formulation of the element matrices for large-displacement/rotation behaviour of a beam with rectangular cross-sectional area is used here for illustration. Using segmentation of the element cross-section as shown in Fig. 1, and allowing some segments to be “void” (with zero mechanical strength and stiffness; zero thermal resistance), the effects of concrete spalling on the thermal and structural behaviours of beam and column members can be modelled. However, the research will

not try to predict or to assess the likely levels of concrete spalling, but will examine the impact, if and when it happens to structural members, on the global performance of concrete structures in fire. This will enable designers to design against the possibility of local or global structural failures as a result of spalling from the surfaces of structural members. The reference axis for a beam-column element, on which the nodes are located, can be placed inside or outside the cross-section of the element. Hence, the elements can easily be combined with shell or plate elements to model reinforced concrete structures in fire. Each of the three nodes of the element has the conventional six degrees of freedom, three translational and three rotational, in both local and global coordinates. The main assumptions of the model can be summarised as follows:

- Plane sections originally normal to the reference axis remain plane and undistorted under deformation, but are not necessarily normal to this axis. It is assumed that there is no slip between segments.
- The displacements and rotations of the element can be arbitrarily large, but the element strains are still assumed to be small, which means that the cross-sectional area does not change. This is an appropriate assumption for most geometrically non-linear analyses of beam-type structures (Bathe 1982).
- Each segment (or “fibre”) within the cross-section can have a different temperature, which is uniform along the element. The initial material properties of each segment may be different, and the stress-strain relationships may change independently for each segment. This assumption has also been used by Capua and Mari (2007) in modelling of reinforced concrete beams in fire.
- Spalled concrete is represented in the same way as voids in the cross-section, by using void segments which have zero mechanical strength and stiffness, and zero thermal resistance. In situations where spalled concrete is held in place, for example within concrete-filled sections, the thermal properties could be retained although the mechanical strength and stiffness are lost.
- For each segment only the longitudinal stress and two shear stresses are non-zero.

Using the natural coordinates  $r$ ,  $s$ ,  $t$ , shown in Fig. 1, the Cartesian coordinates of a point within a 3-noded element at time  $t'$  are given by

$$\begin{aligned}
{}^t x(r, s, t) &= \sum_{k=1}^3 h_k {}^t x^k + \sum_{k=1}^3 \left( \frac{t a_k}{2} + \Delta t^k \right) h_k {}^t V_{tx}^k + \sum_{k=1}^3 \left( \frac{s b_k}{2} + \Delta s^k \right) h_k {}^t V_{sx}^k \\
{}^t y(r, s, t) &= \sum_{k=1}^3 h_k {}^t y^k + \sum_{k=1}^3 \left( \frac{t a_k}{2} + \Delta t^k \right) h_k {}^t V_{ty}^k + \sum_{k=1}^3 \left( \frac{s b_k}{2} + \Delta s^k \right) h_k {}^t V_{sy}^k \\
{}^t z(r, s, t) &= \sum_{k=1}^3 h_k {}^t z^k + \sum_{k=1}^3 \left( \frac{t a_k}{2} + \Delta t^k \right) h_k {}^t V_{tz}^k + \sum_{k=1}^3 \left( \frac{s b_k}{2} + \Delta s^k \right) h_k {}^t V_{sz}^k
\end{aligned} \tag{1}$$

in which  $h_k(r)$  is the parabolic shape function used for the three-noded beam element, expressed as

$$h_1 = \frac{1}{2}(1-r) - \frac{1}{2}(1-r^2), \quad h_2 = \frac{1}{2}(1+r) - \frac{1}{2}(1-r^2), \quad h_3 = (1-r^2)$$

Using Equation (1) the expressions for the total displacements ( $u, v, w$ ) and their incremental components ( $\Delta u, \Delta v, \Delta w$ ), in terms of the nodal point values and changes in the direction cosines of the nodal point vectors, can be written as:

$$\begin{aligned}
{}^t u(r, s, t) &= \sum_{k=1}^3 h_k {}^t u^k + \sum_{k=1}^3 \left( \frac{t a_k}{2} + \Delta t^k \right) h_k ({}^t V_{tx}^k - {}^0 V_{tx}^k) + \sum_{k=1}^3 \left( \frac{s b_k}{2} + \Delta s^k \right) h_k ({}^t V_{sx}^k - {}^0 V_{sx}^k) \\
{}^t v(r, s, t) &= \sum_{k=1}^3 h_k {}^t v^k + \sum_{k=1}^3 \left( \frac{t a_k}{2} + \Delta t^k \right) h_k ({}^t V_{ty}^k - {}^0 V_{ty}^k) + \sum_{k=1}^3 \left( \frac{s b_k}{2} + \Delta s^k \right) h_k ({}^t V_{sy}^k - {}^0 V_{sy}^k) \\
{}^t w(r, s, t) &= \sum_{k=1}^3 h_k {}^t w^k + \sum_{k=1}^3 \left( \frac{t a_k}{2} + \Delta t^k \right) h_k ({}^t V_{tz}^k - {}^0 V_{tz}^k) + \sum_{k=1}^3 \left( \frac{s b_k}{2} + \Delta s^k \right) h_k ({}^t V_{sz}^k - {}^0 V_{sz}^k)
\end{aligned} \tag{2}$$

and

$$\begin{aligned}
\Delta u(r, s, t) &= \sum_{k=1}^3 h_k \Delta u^k + \sum_{k=1}^3 \left( \frac{t a_k}{2} + \Delta t^k \right) h_k V_{tx}^k + \sum_{k=1}^3 \left( \frac{s b_k}{2} + \Delta s^k \right) h_k V_{sx}^k \\
\Delta v(r, s, t) &= \sum_{k=1}^3 h_k \Delta v^k + \sum_{k=1}^3 \left( \frac{t a_k}{2} + \Delta t^k \right) h_k V_{ty}^k + \sum_{k=1}^3 \left( \frac{s b_k}{2} + \Delta s^k \right) h_k V_{sy}^k \\
\Delta w(r, s, t) &= \sum_{k=1}^3 h_k \Delta w^k + \sum_{k=1}^3 \left( \frac{t a_k}{2} + \Delta t^k \right) h_k V_{tz}^k + \sum_{k=1}^3 \left( \frac{s b_k}{2} + \Delta s^k \right) h_k V_{sz}^k
\end{aligned} \tag{3}$$

in which,

$$\begin{cases}
V_{tx}^k = {}^{t+\Delta t'} V_{tx}^k - {}^t V_{tx}^k \\
V_{ty}^k = {}^{t+\Delta t'} V_{ty}^k - {}^t V_{ty}^k \\
V_{tz}^k = {}^{t+\Delta t'} V_{tz}^k - {}^t V_{tz}^k \\
V_{sx}^k = {}^{t+\Delta t'} V_{sx}^k - {}^t V_{sx}^k \\
V_{sy}^k = {}^{t+\Delta t'} V_{sy}^k - {}^t V_{sy}^k \\
V_{sz}^k = {}^{t+\Delta t'} V_{sz}^k - {}^t V_{sz}^k
\end{cases} \tag{4}$$

The relationship given in Equation (2) is directly employed to evaluate the total displacements and total strains (hence also the total stresses) and holds for any magnitude of the displacement components. The relationship of Equation (3) is used in the linearization of the Principle of Virtual Work, and needs to express the components of the changes in the direction cosines  $\mathbf{V}_t^k$  and  $\mathbf{V}_s^k$  in terms of the nodal rotational degrees of freedom. Depending on the size of the incremental step, the actual rotations corresponding to the vectors  $\mathbf{V}_t^k$ ,  $\mathbf{V}_s^k$  may be large, and therefore cannot be represented by vector component rotations about the Cartesian axes. However, the objective here is to express the continuum linear and non-linear strain increments using the finite element degrees of freedom and the corresponding interpolations, so as to achieve a full linearization of the Principle of Virtual Work. The vector of nodal rotational degrees of freedom  $\boldsymbol{\theta}_k$  can be defined using the components measured about the Cartesian axes, using the second-order approximations (Bathe 1996),

$$\begin{cases} \mathbf{V}_t^k = \boldsymbol{\theta}_k \times {}^t\mathbf{V}_t^k + \frac{1}{2}\boldsymbol{\theta}_k \times (\boldsymbol{\theta}_k \times {}^t\mathbf{V}_t^k) \\ \mathbf{V}_s^k = \boldsymbol{\theta}_k \times {}^t\mathbf{V}_s^k + \frac{1}{2}\boldsymbol{\theta}_k \times (\boldsymbol{\theta}_k \times {}^t\mathbf{V}_s^k) \end{cases} \quad (5)$$

where,

$$\boldsymbol{\theta}_k \times {}^t\mathbf{V}_t^k = \begin{Bmatrix} \theta_y^k {}^tV_{tz}^k - \theta_z^k {}^tV_{ty}^k \\ \theta_z^k {}^tV_{tx}^k - \theta_x^k {}^tV_{tz}^k \\ \theta_x^k {}^tV_{ty}^k - \theta_y^k {}^tV_{tx}^k \end{Bmatrix} \quad (6)$$

and

$$\boldsymbol{\theta}_k \times {}^t\mathbf{V}_s^k = \begin{Bmatrix} \theta_y^k {}^tV_{sz}^k - \theta_z^k {}^tV_{sy}^k \\ \theta_z^k {}^tV_{sx}^k - \theta_x^k {}^tV_{sz}^k \\ \theta_x^k {}^tV_{sy}^k - \theta_y^k {}^tV_{sx}^k \end{Bmatrix} \quad (7)$$

The only purpose of using  $\boldsymbol{\theta}_k$  is to evaluate (approximations to) the new direction vectors;  $\boldsymbol{\theta}_k$  is discarded thereafter.

Equations (1) to (5) are the basic interpolations and expressions which are used to establish the strain-displacement interpolation matrices for geometrically non-linear analysis. In this study a Total Lagrangian (TL) formulation is adopted.

## Element stiffness matrix

Based on the formulations proposed by Bathe (1982) the linear strain-displacement transformation matrix can be written as,

$$\Delta\boldsymbol{\varepsilon} = \begin{Bmatrix} \Delta\varepsilon_{x'} \\ \Delta\gamma_{x'y'} \\ \Delta\gamma_{z'x'} \end{Bmatrix} = {}^{t'}_0\bar{\mathbf{B}}_L \Delta\hat{\mathbf{u}} \quad (8)$$

where,  $\Delta\hat{\mathbf{u}}$  is the displacement increment vector in global coordinates  $(x, y, z)$ .

The linear strain-displacement transformation matrix  ${}^{t'}_0\bar{\mathbf{B}}_L$  relates the displacement increment  $\Delta\hat{\mathbf{u}}$  in global coordinates, to the strain increment  $\Delta\boldsymbol{\varepsilon}$  in local coordinates  $(x', y', z')$ , and can be expressed as

$${}^{t'}_0\bar{\mathbf{B}}_L = {}^0\mathbf{T} {}^{t'}_0\mathbf{B}_L \quad (9)$$

where  ${}^{t'}_0\mathbf{B}_L$  is the linear strain-displacement transformation matrix in global coordinates at time  $t'$  and  ${}^0\mathbf{T}$  is the transformation matrix related to the initial configuration,

and

$${}^{t'}_0\mathbf{B}_L = {}^{t'}_0\mathbf{B}_{L0} + {}^{t'}_0\mathbf{B}_{L1} \quad (10)$$

The detailed construction of  ${}^{t'}_0\mathbf{B}_{L0}$ ,  ${}^{t'}_0\mathbf{B}_{L1}$  and  ${}^0\mathbf{T}$  has been given by Huang *et al.* (2003b).

The non-linear strain-displacement transformation matrix  ${}^{t'}_0\bar{\mathbf{B}}_{NL}$ , in local coordinates, can be expressed as

$${}^{t'}_0\bar{\mathbf{B}}_{NL} = {}^0\tilde{\mathbf{T}}^T {}^{t'}_0\mathbf{B}_{NL} \quad (11)$$

where  ${}^{t'}_0\mathbf{B}_{NL}$  is the non-linear strain-displacement transformation matrix in global coordinates at time  $t'$  and  ${}^0\tilde{\mathbf{T}}$  is the transformation matrix relative to the initial configuration.

The detailed structure of  ${}^{t'}_0\mathbf{B}_{NL}$  and  ${}^0\tilde{\mathbf{T}}$  has been given by Huang *et al.* (2003b).

The 2<sup>nd</sup> Piola-Kirchhoff stress matrix in local coordinates can be expressed as

$${}^{t'}_0\bar{\mathbf{S}} = \begin{bmatrix} {}^{t'}_0\tilde{\mathbf{S}} & \mathbf{0} & \mathbf{0} \\ \mathbf{0} & {}^{t'}_0\tilde{\mathbf{S}} & \mathbf{0} \\ \mathbf{0} & \mathbf{0} & {}^{t'}_0\tilde{\mathbf{S}} \end{bmatrix} \quad (12)$$

where,

$${}^t_0 \tilde{\mathbf{S}} = \begin{bmatrix} {}^t_0 \mathbf{S}_{x'x'} & {}^t_0 \mathbf{S}_{x'y'} & {}^t_0 \mathbf{S}_{x'z'} \\ {}^t_0 \mathbf{S}_{x'y'} & 0 & 0 \\ {}^t_0 \mathbf{S}_{x'z'} & 0 & 0 \end{bmatrix} \quad (13)$$

and 2<sup>nd</sup> Piola-Kirchhoff stress vector is

$${}^t_0 \widehat{\mathbf{S}} = \begin{bmatrix} {}^t_0 \mathbf{S}_{x'x'} \\ {}^t_0 \mathbf{S}_{x'y'} \\ {}^t_0 \mathbf{S}_{x'z'} \end{bmatrix} = \mathbf{D}' \left( {}^t_0 \boldsymbol{\varepsilon} - {}^t \boldsymbol{\varepsilon}_T - {}^t \boldsymbol{\varepsilon}_{tr} \right) \quad (14)$$

where  $\mathbf{D}'$  is the material constitutive matrix,

$$\mathbf{D}' = \begin{bmatrix} E_t & 0 & 0 \\ 0 & kG & 0 \\ 0 & 0 & kG \end{bmatrix} \quad (15)$$

where  $k=5/6$  is the shear correction factor (Bathe (1982)). For 'void' segments  $\mathbf{D}' = \mathbf{0}$ .

In Equation (14)  ${}^t \boldsymbol{\varepsilon}_T$  and  ${}^t \boldsymbol{\varepsilon}_{tr}$  are the vectors of total thermal strain and total transient state strain of concrete (for reinforcing steel segments  ${}^t \boldsymbol{\varepsilon}_{tr} = \mathbf{0}$ ) and the current total strains  ${}^t_0 \boldsymbol{\varepsilon}$  are now the Green-Lagrange strains which can be calculated as:

$${}^t_0 \boldsymbol{\varepsilon} = {}^{t'-\Delta t'}_0 \boldsymbol{\varepsilon} + \Delta \boldsymbol{\varepsilon} \quad (16)$$

The incremental strains  $\Delta \boldsymbol{\varepsilon}$  can be calculated using Equation (8), and it is assumed that the thermal expansion and transient state strain produce zero shear strains, so that the shear terms in the vectors of  ${}^t \boldsymbol{\varepsilon}_T$  and  ${}^t \boldsymbol{\varepsilon}_{tr}$  vanish. The values of stress and stiffness at each Gauss point for each segment can therefore be determined.

The element stiffness matrix  $\mathbf{K}_T$  can be expressed as

$$\mathbf{K}_T = {}^t_0 \mathbf{K}_L + {}^t_0 \mathbf{K}_{NL} \quad (17)$$

Using the Principle of Virtual Work,

$$\begin{aligned} {}^t_0 \mathbf{K}_L &= \int_{0_V} {}^t_0 \overline{\mathbf{B}}_L^T \mathbf{D}' {}^t_0 \overline{\mathbf{B}}_L d^0V \\ &= \iiint_{0_V} {}^t_0 \overline{\mathbf{B}}_L^T \mathbf{D}' {}^t_0 \overline{\mathbf{B}}_L d^0x d^0y d^0z \\ &= \iiint_{0_{V^*}} {}^t_0 \overline{\mathbf{B}}_L^T \mathbf{D}' {}^t_0 \overline{\mathbf{B}}_L \det |\mathbf{J}| dr ds dt \end{aligned} \quad (18)$$

and

$$\begin{aligned}
{}^t_0 \mathbf{K}_{NL} &= \int_{0_V} {}^t_0 \overline{\mathbf{B}}_{NL}^T {}^t_0 \overline{\mathbf{S}} {}^t_0 \overline{\mathbf{B}}_{NL} d^0V \\
&= \iiint_{0_V} {}^t_0 \overline{\mathbf{B}}_{NL}^T {}^t_0 \overline{\mathbf{S}} {}^t_0 \overline{\mathbf{B}}_{NL} d^0x d^0y d^0z \\
&= \iiint_{0_{V^*}} {}^t_0 \overline{\mathbf{B}}_{NL}^T {}^t_0 \overline{\mathbf{S}} {}^t_0 \overline{\mathbf{B}}_{NL} \det |\mathbf{J}| dr ds dt
\end{aligned} \tag{19}$$

The objective here is to develop a beam-column formulation which is suitable for modelling of reinforced concrete structures subject to fire conditions, and so the cross-section of each element is divided into segments to allow variation of the distributions of temperature, stress and strain over the cross-section (see Fig. 2) to take place. Hence, the element stiffness matrix can be calculated using Gaussian integration along the length of the beam-column element (the  $r$ -direction) in which two integration points are adopted for a three-noded element. The integration over the cross-section of the element is performed by simple summation of the contributions from the segments into which the cross-section is divided. Hence, Equation (18) can be expressed as

$$\begin{aligned}
{}^t_0 \mathbf{K}_L &= \iiint_{0_{V^*}} {}^t_0 \overline{\mathbf{B}}_L^T \mathbf{D} {}^t_0 \overline{\mathbf{B}}_L \det |\mathbf{J}| dr ds dt \\
&= \int_r {}^t_0 \overline{\mathbf{K}}_L(r) dr \\
&= \alpha_1 [{}^t_0 \overline{\mathbf{K}}_L(r_1)] + \alpha_2 [{}^t_0 \overline{\mathbf{K}}_L(r_2)]
\end{aligned} \tag{20}$$

in which the integration weighting factors are  $\alpha_1 = \alpha_2 = 1.0$ , and

$$\begin{aligned}
{}^t_0 \overline{\mathbf{K}}_L(r) &= \iint_{0_{A^*}} {}^t_0 \overline{\mathbf{B}}_L^T \mathbf{D} {}^t_0 \overline{\mathbf{B}}_L \det |\mathbf{J}| ds dt \\
&= \sum_{n=1}^M \left( [{}^t_0 \overline{\mathbf{B}}_L(n)]^T \mathbf{D}_n [{}^t_0 \overline{\mathbf{B}}_L(n)] \det |\mathbf{J}(n)| \right) \Delta s_n \Delta t_n
\end{aligned} \tag{21}$$

where,  $n$  is the number of a segment, and  $M$  is the total number of segments within the cross-section.

From Equation (19)

$$\begin{aligned}
{}^t_0 \mathbf{K}_{NL} &= \iiint_{0_{V^*}} {}^t_0 \overline{\mathbf{B}}_{NL}^T {}^t_0 \overline{\mathbf{S}} {}^t_0 \overline{\mathbf{B}}_{NL} \det |\mathbf{J}| dr ds dt \\
&= \int_r [{}^t_0 \overline{\mathbf{K}}_{NL}(r)] dr \\
&= \alpha_1 [{}^t_0 \overline{\mathbf{K}}_{NL}(r_1)] + \alpha_2 [{}^t_0 \overline{\mathbf{K}}_{NL}(r_2)]
\end{aligned} \tag{22}$$

in which once again  $\alpha_1 = \alpha_2 = 1.0$ , with

$$\begin{aligned}
{}^t_0 \overline{\mathbf{K}}_{NL}(r) &= \iint_{0_{A^*}} {}^t_0 \overline{\mathbf{B}}_{NL}^T {}^t_0 \overline{\mathbf{S}} {}^t_0 \overline{\mathbf{B}}_{NL} \det |\mathbf{J}| ds dt \\
&= \sum_{n=1}^M \left( [{}^t_0 \overline{\mathbf{B}}_{NL}(n)]^T {}^t_0 \overline{\mathbf{S}}(n) [{}^t_0 \overline{\mathbf{B}}_{NL}(n)] \det |\mathbf{J}(n)| \right) \Delta s_n \Delta t_n
\end{aligned} \tag{23}$$

Using Equation (17) the element stiffness matrix  $\mathbf{K}_T$  can be determined.

## Element internal force vector

Using the same principle used to form the element stiffness matrix the element internal force vector,  ${}^t_0 \mathbf{F}$ , can be calculated as follows:

$$\begin{aligned}
 {}^t_0 \mathbf{F} &= \int_{0_V} {}^t_0 \overline{\mathbf{B}}_L^T {}^t_0 \overline{\hat{\mathbf{S}}} d^0V \\
 &= \iiint_{0_V} {}^t_0 \overline{\mathbf{B}}_L^T {}^t_0 \overline{\hat{\mathbf{S}}} d^0x d^0y d^0z \\
 &= \iiint_{0_V^*} {}^t_0 \overline{\mathbf{B}}_L^T {}^t_0 \overline{\hat{\mathbf{S}}} \det|\mathbf{J}| dr ds dt
 \end{aligned} \tag{24}$$

Carrying out numerical integration on (24), in the same way as in forming the element stiffness matrix, the element internal force vector can be written as

$$\begin{aligned}
 {}^t_0 \mathbf{F} &= \iiint_{0_V^*} {}^t_0 \overline{\mathbf{B}}_L^T {}^t_0 \overline{\hat{\mathbf{S}}} \det|\mathbf{J}| dr ds dt \\
 &= \int_{0_r} [{}^t_0 \overline{\mathbf{F}}(r)] dr \\
 &= \alpha_1 [{}^t_0 \overline{\mathbf{F}}(r_1)] + \alpha_2 [{}^t_0 \overline{\mathbf{F}}(r_2)]
 \end{aligned} \tag{25}$$

where,  $\alpha_1 = \alpha_2 = 1.0$  and

$$\begin{aligned}
 {}^t_0 \overline{\mathbf{F}}(r) &= \iint_{0_A^*} {}^t_0 \overline{\mathbf{B}}_L^T {}^t_0 \overline{\hat{\mathbf{S}}} \det|\mathbf{J}| ds dt \\
 &= \sum_{n=1}^M [{}^t_0 \overline{\mathbf{B}}_L(n)]^T [{}^t_0 \overline{\hat{\mathbf{S}}}(n)] \det|\mathbf{J}(n)| \Delta s_n \Delta t_n
 \end{aligned} \tag{26}$$

## CONSTITUTIVE MODELLING AND PROPERTIES OF MATERIALS

The stress-strain relationships of concrete at elevated temperatures specified by EN 1992-1-2 (2004) are adopted for this study. The uniaxial tensile and compressive strengths of concrete (in MPa) are assumed to be related by  $f'_t = 0.3321 \sqrt{f'_c}$  (ASCE 1982). Hence the concrete tensile strength  $f'_t$  changes with temperature. It is assumed that concrete exhibits linearly elastic behaviour up to its ultimate tensile capacity. Beyond this point the concrete cracks and the tensile stress decreases gradually with increasing tensile strain, rather than dropping to zero abruptly as would occur in a perfectly brittle material. This phenomenon is known as tensile strain-softening. In this study the bi-linear curve suggested by Rots *et al.* (1984), which is shown in Fig. 3, has been used to model tensile strain-softening. In this figure  $\varepsilon_{cr} = f'_t / E_c$ ,  $\varepsilon_{cu} = \alpha_1 \varepsilon_{cr}$  and  $\alpha_1 = 10 \sim 25$  (Barzegar-Jamshidi 1987). The constitutive matrix  $\mathbf{D}'_c$  of a cracked concrete segment becomes

$$\mathbf{D}'_c = \begin{bmatrix} 0 & 0 & 0 \\ 0 & \mu G_c & 0 \\ 0 & 0 & \mu G_c \end{bmatrix} \quad (27)$$

where  $G_c$  is the shear modulus of concrete and  $\mu$  is the shear retention factor for which  $0 < \mu \leq 1.0$ . After crushing, the concrete is assumed to lose all strength and stiffness. For reinforcing steel the stress-strain curves at elevated temperatures suggested by EN 1992-1-2 (2004) has been adopted in this study.

The Transient State Strain (TSS) of concrete is the strain that cannot otherwise be accounted for due to the decomposition of the cement paste. It occurs under compressive stress as temperature increases, is essentially permanent, unrecoverable and only occurs under initial heating. TSS is temperature-dependent and independent of time. Previous researchers (Anderberg and Thelandersson 1976; Khoury *et al.* 1985) have indicated that the effects of TSS on the structural behaviour of reinforced concrete structures, especially concrete columns, in fire may be significant. In this work, the model proposed by Anderberg and Thelandersson (1976) is adopted to calculate uniaxial TSS of concrete,  $\varepsilon_{tr}$ , which is described as

$$\Delta\varepsilon_{tr} = -k_2 \frac{\sigma_c}{f'_{c,0}} \Delta\varepsilon_T \quad 20 \leq T < 500^\circ\text{C} \quad (28)$$

where,  $\Delta\varepsilon_T$  is increment of thermal strain,  $f'_{c,0}$  is compressive strength of concrete at ambient condition and  $k_2$  is a dimensionless constant varying with cement type. Anderberg and Thelandersson found by linear regression that a value of  $k_2 = 2.35$  best described the quartzite concrete used in their tests. This value has been used in this research.

For temperatures above  $500^\circ\text{C}$  TSS accelerates considerably. Anderberg proposed the following expression for the incremental change in  $\varepsilon_{tr}$ :

$$\Delta\varepsilon_{tr} = -0.1 \times 10^{-3} \Delta T \frac{\sigma_c}{f'_{c,0}} \quad T \geq 500^\circ\text{C} \quad (29)$$

where  $\Delta T$  is the temperature increment during step  $i$ .

The total TSS at step  $n$  is then calculated as follows:

$$\varepsilon_{tr}(n) = \sum_{i=1}^n \Delta\varepsilon_{tr}(i) \quad (30)$$

Transient state shear strains are ignored for simplicity. Therefore the TSS vector is expressed as

$${}^t \boldsymbol{\varepsilon}_{tr} = \begin{Bmatrix} \boldsymbol{\varepsilon}_{tr}(n) \\ 0 \\ 0 \end{Bmatrix} \quad (31)$$

Since TSS is considered as irrecoverable and only occur under initial heating, in this study the TSS is assumed to remain unchanged and equal to the value attained at the maximum temperature of the concrete, which is usually reached during the cooling period of the fire. In this study, thermal elongations of concrete and reinforcing steel are calculated on the basis of the models suggested by EN 1992-1-2 (2004).

The above developments have been incorporated into *Vulcan* in order to model the structural behaviour of reinforced concrete buildings in fire conditions. The total loading or temperature rise for which the response of the structure is to be traced is divided into a number of steps. It is assumed that changes in the loads or temperatures occur only at the beginning or end of a step. During any step the external loads and temperatures in the segments of all elements are assumed to remain unchanged.

## VALIDATIONS

### Geometric non-linearity and segmentation of cross-section

Some simple example studies are now presented in order to illustrate the capabilities of the new beam-column element and its sensitivity to cross-section segmentation and element meshing. A simply supported linear-elastic beam ( $E = 210 \text{ GPa}$ ,  $\nu = 0.0$ ) with I-section (thickness of top and bottom flanges = 10mm; thickness of web = 20mm) was analysed when subject to a mid-span point load at ambient temperature. As shown in Fig. 4 the beam has been modelled using void and solid segments in its cross-section segment matrix to create the I-section shape.

The first case addressed the effect of *cross-section segmentation*. A beam of 4m span was modelled using four elements. Four levels of cross-section segmentation with between 9 and 400 segments (3x3, 5x5, 10x10, and 20x20) were adopted in the analyses. Fig. 5 shows a comparison of the predictions from models with different segmentation, together with a closed-form calculation using geometrically non-linear beam theory (Gere and Timoshenko 1990). It is evident that the results predicted using relatively coarse segmentation (5x5) are almost identical to the finest (20x20) and agree very well with the geometrically non-linear beam theory. This illustrates the basic efficiency of the segmentation approach proposed in this paper in modelling different cross-section shapes.

In order to investigate *finite element* mesh sensitivity the beam length was modelled by using 1, 2, 4, and 16 elements, for all of which the cross-section of the beam was divided into 10x10 segments.

The results are shown in Fig. 6. It is evident that the absolute value of the discrepancy between the model's prediction and the calculation using geometrically non-linear beam theory is monotonically reduced as the element number increased. It is clear that the results predicted using 4 and 16 elements are almost identical. There were only small discrepancies between these and the results of the 2 and 4 element models. The study indicated that the model developed here is quite robust in being relatively insensitive to both segment and element meshing for material linear elastic beam. However, for reinforced concrete beam-column members in fire it is necessary to use a high degree of segmentation in order to represent some temperature distributions and material properties adequately. From the authors' experience it is recommended that the size of the concrete segments in the areas closed to the fire boundary should be limited to less than 10mm, and the size of the concrete segments in the areas away from the fire boundary should not exceed 40mm. It is evident that the procedure can be used to deal with very high displacements, considerably beyond the range which would be encountered in real structural fire engineering examples.

### **High-strength concrete columns in fire**

Ali *et al.* (2001) conducted a series of furnace tests on high-strength concrete columns. Their tests showed severe spalling on some tested columns. Two heating regimes, characterised as 'high' and 'low' heating, were adopted in the tests. The high-heating furnace temperature followed the BS476 standard fire curve. The tested columns each had 127x127mm cross-section and 1800mm height. Each column was reinforced with four 12mm diameter main steel bars, with a concrete cover of 25mm. According to BS 8110 (1997), the design strength of all of these columns was 804kN. In the tests the column was held inside the furnace between hinged supports at the top and bottom. At the age of 100 days the average concrete strength was 119 MPa, and its moisture content was 5.5% by weight. These data were used in this study.

Two column tests (designated HH15 and HH17) are modelled in this paper to validate the non-linear procedure developed. Both columns were subject to a loading level of 60% of the design strength, and this was kept constant during the fire tests. Columns HH15 and HH17 were subject to 'high heating' and 'low' heating, respectively. From the test evidence, major spalling happened at around 15min into the test for column HH15. The mass of concrete lost due to spalling was 16% of original mass of the column, which is equivalent to losing an average of 5.4mm of the concrete cover from all the surfaces of the column. Because there are no records from the tests to indicate the concrete spalling position and severity along the length of columns tested; in the model it was therefore assumed that after 15min of the test a 5.4mm thick concrete layer was removed from the column. This approximation may not be conservative if some localised concrete spalling happened during the tests. Hence the thermal and structural responses of the column were changed

dramatically from this stage onwards. However, column HH17 suffered very little concrete spalling during the test, and hence it was modelled without concrete spalling.

The first step of the analysis is to perform a thermal analysis on the columns modelled. *Vulcan* has recently been extended to include a two-dimensional non-linear finite element procedure to predict the temperature distributions within the cross-sections of structural members subject to given fire time-temperature regimes. This is largely based on previous work (Huang *et al.* 1996) by the first author. The thermal properties of the steel and concrete are assumed to change with temperature, and the influence of moisture initially held within the concrete has been taken into account. In this analysis the thermal properties given in EN 1992-1-2 (2004) for concrete and steel have been adopted. In order to consider the effect of surface spalling on the thermal behaviour of the columns, modifications were made to *Vulcan* to allow inner layers of the cross-section to be exposed directly to fire after the outer concrete layer has spalled. Hence the affect of surface spalling on the temperature distributions within cross-sections is modelled. In this study the cross-section of the columns were divided into 20x20 segments in which the sizes of the segments were varied from 5.4mm to 30mm. Hence, a total of 400 segments have been used to represent the cross-sections of the columns. The spalled concrete layer was represented by the segments with 5.4mm thickness. The predicted temperatures of the main steel bars for both columns are shown in Fig. 7, together with the test measurements. It is evident that the predictions and test results are in remarkably good agreement.

The predicted temperatures were then used to perform structural analysis for the test columns, the mesh which had been used for thermal analysis also being used for segmentation of the cross-sections of the columns. Because a model of TSS is not available for high-strength concrete, the model developed by Anderberg and Thelandersson (1976) for normal-strength concrete was used in this analysis. In order to assess the effect of TSS on the column behaviour, three levels (100%, 75% and 50% of the TSS calculated using Anderberg's model) were used in the modelling. Figs. 8 and 9 show the comparisons of predicted and tested axial displacements against test time for columns HH15 and HH17. It is evident that the effect of TSS on the axial displacement can be very significant. However, there is very little influence on the failure times of these columns, and the predicted failure times agree well with the test results for both columns. For HH15 the axial displacements, caused mainly by thermal expansion, dropped suddenly at 15 minutes test time due to spalling of the 5.4mm thick surface layer of the concrete. The outer layer of the concrete, in which the temperatures were much higher than those in the inner part of the cross-section, was the main contributor to the average thermal expansion of the column.

In order to assess the effect of spalling on the behaviour of both columns, HH15 was re-analysed without considering spalling and column HH17 was simulated with 5.4mm of surface layer spalling at 15 minutes test time. TSS was assumed as 75% of the value calculated using Anderberg's model for both analyses. The results are presented in Figs. 10 and 11. It is evident that the impact of surface spalling on the behaviour of both columns is very significant. The fire resistance times of columns HH15 and column HH17 were reduced by 22% and 17%, respectively for only 5.4mm surface spalling of the concrete.

### **Normal-strength concrete beams in fire**

Lin *et al.* (1987) conducted a series of fire tests on normal-strength reinforced concrete beams for which two heating curves, the ASTM fire and Short Duration High Intensity (SDHI) fire, were adopted. In order to demonstrate the capability of the proposed model four beams, designated Beams 1, 3, 5 and 6, were modelled. Beams 1 and 3 were heated using the ASTM fire and Beams 5 and 6 were subjected to the SDHI fire. As for the modelling of columns, the thermal analysis on the beams were carried out first, with division of their cross-sections into 28x16 with a total of 448 segments for both thermal and structural analyses.

Fig. 12 provides details of Beams No. 1 3, 5 and 6. The load  $P$  was kept constant at 44.48 kN during each fire test, although the cantilever force  $P_0$  varied as the test progressed. The measured values of  $P_0$  for the beams and the test values of material properties at room temperature were used for this study. These data were also employed by Lin, *et al.* (1987) for their structural analytical results. No significant concrete spalling was reported for the tests, and therefore all the beams were modelled without considering spalling in this validation. Since the beams were constructed using normal-strength concrete, TSS was calculated using Anderberg's model. Thermal analyses were conducted to predict temperature histories within the beam cross-sections. As shown in Fig. 12, there are four layers of main reinforcing steel within the cross-sections. In presenting the results of the thermal analyses, the reinforcing steel layers are denoted in sequence from bottom to top as Layers 1 to 4. The predicted temperature histories of the main reinforcing steel layers for Beams 1 and 5, which were subsequently used for structural analysis, are shown in Figs 13 and 14, together with those test results which are available. It is evident that reasonable agreement has been achieved between test and prediction.

In order to quantify the effect of TSS on simple beam members in fire conditions, the four beams were modelled with and without TSS. The predictions of the current model, for Beams 1 and 3 heated by the ASTM fire and Beams 5 and 6 by the SDHI fire, are presented in Figs 15 to 18, together with test results and the results predicted by Lin *et al.* (1987). It is evident that the current

model agrees well with the test results for Beams 1 and 3, and achieves reasonable accuracy for Beams 5 and 6. Once again TSS has a significant affect on deflection of the beams, but very little on their failure times; this is evident from Figs 15 and 16.

Previous researches have indicated that concrete spalling is very likely to happen before 30 minutes of an ISO834 fire test. To demonstrate the influence that spalling would have on the behaviour of Beam 1, it is now assumed as Case 1 that a 7.5mm thick surface layer exposed to fire is removed at 25 min test time. As Case 2 it is assumed that the same spalling happens at 25 min test time, and that a further 10mm thick layer of concrete is subsequently removed at 35 min test time. The temperature histories of the bottom layer of reinforcing steel for these two cases are shown in Fig. 19, from which it is evident that the effect of spalling on the temperature of reinforcement is very significant. The maximum deflections of the beams for both cases are shown in Fig. 20. In Case 1 the fire resistance of the spalled beam is reduced by about 40 minutes. For Case 2, the fire resistance is reduced by 64 minutes. Beam 3 was also analysed, assuming that a 10mm thick surface layer of concrete exposed to fire is removed at 25 min test time for Case 1. For Case 2 it is assumed that a 10mm thick of surface layer of concrete spalls at 25 min test time, and a further 15mm thick layer is removed at 35 min test time. Fig. 21 shows the results of these two cases, showing that the fire resistances of both cases are significantly reduced.

## CONCLUSIONS

In this paper a robust non-linear finite element procedure has been developed for modelling of reinforced concrete beam and column structures in fire. In this formulation both geometric and material non-linearities have been taken into account. The cross-section of the beam-column element is divided into a number of segments, each of which can have different material, temperature and mechanical properties. The more complex aspects of structural behaviour in fire conditions, such as thermal expansion, transient state strains in the concrete, cracking or crushing of concrete, yielding of steel and change of material properties with temperature, are modelled. By allowing void segments the effect of concrete spalling in fire can be modelled effectively by this model. Hence, a quantitative assessment of the residual strength of spalled reinforced concrete beam-column structures in fire can be made using the model developed in this paper. Since the elements possess an offset capability, these elements can also be used, with shell or plate elements, for modelling of reinforced concrete buildings in fire. A series of validations have been conducted to validate the model. It is evident that the proposed model can be used to predict the fire resistance of reinforced concrete beam-column structures, taking into account the effect of concrete spalling. From this research it can be concluded that the influence of transient state strains of concrete on the

deflection of a structure is significant. However, there is very little effect on the failure times of these simple structural members. The effects of surface spalling on both the thermal and structural behaviour of reinforced concrete members are very significant. It is vitally important to consider the likelihood and the effects of spalling in the performance-based fire-safe design of reinforced concrete buildings. This should logically be reflected in future design codes.

## REFERENCES

- Ali, F.A., O'Connor, D. and Abu-Tair, A. (2001), "Explosive Spalling of High-Strength Concrete Columns in Fire", *Magazine of Concrete Research*, **53** (3), 197-204.
- American Society of Civil Engineers (1982), "*Finite Element Analysis of Reinforced Concrete*", ASCE, New York.
- Anderberg Y. and Thelandersson S. (1976), "*Stress and Deformation Characteristics of Concrete at High Temperatures, 2 Experimental Investigation and Material Behaviour Model*", Lund Institute of Technology, Bulletin 54, Lund, Sweden.
- Bailey C.G., Burgess I.W. and Plank R.J. (1996), "Computer Simulation of a Full-Scale Structural Fire Test", *The Structural Engineer*, **74** (6), 93-100.
- Barzegar-Jamshidi F. (1987), "Non-Linear Finite Element Analysis of Reinforced Concrete under Short Term Monotonic Loading", PhD Thesis, University of Illinois at Urbana-Champaign.
- Bathe K.J., Bolourchi S. (1979), "Large Displacement Analysis of Three-Dimensional Beam Structures", *International Journal for Numerical Methods in Engineering*, **14**, 961-986.
- Bathe K.J. (1982), "*Finite Element Procedures in Engineering Analysis*", Prentice-Hall Inc., New Jersey.
- Bathe K.J. (1996), "*Finite Element Procedures*", Prentice-Hall Inc., New Jersey.
- Bratina S., Saje M. and Planinc I. (2007), "The Effects of Different Strain Contributions on The Response of RC Beams in Fire" *Engineering Structures*, **29**, 418-430.
- BS 8110-1 (1997), "*Structural Use of Concrete- Part 1: Code of Practice for Design and Construction*", BSI.
- Capua D. D. and Mari A. R. (2007), "Non-linear Analysis of Reinforced Concrete Cross-Sections Exposed to Fire", *Fire Safety Journal*, **42**, 139-149.
- Cai J., Burgess I. W. and Plank R. J. (2002), "Modelling of Asymmetric Cross-Section Members for Fire Conditions", *Journal of Constructional Steel Research*, **58**, 389-412.
- Ellingwood B., and Lin T.D. (1991), "Flexure and Shear Behaviour of Concrete Beams During Fires", *Journal of Structural Engineering, ASCE*, **117** (2), 440-458.

- EN 1992-1-2 (2004), “Eurocode 2, Design of Concrete Structures, Part 1.2: General Rules - Structural Fire Design”, Commission of the European Communities, Brussels.
- EN 1994-1-2 (2005), “Eurocode 4, Design of Composite Steel and Concrete Structures, Part 1.2: General rules - Structural Fire Design”, Commission of the European Communities, Brussels.
- Gere J.M. and Timoshenko S.P. (1990), “Mechanics of Materials”, Third Edition, PWS-KENT Publishing Company.
- Huang Z., Platten A. and Roberts J. (1996), “Non-linear Finite Element Model to Predict Temperature Histories within Reinforced Concrete in Fires”, *Building and Environment*, **31**(2), 109-118.
- Huang Z. and Platten A. (1997), “Non-linear Finite Element Analysis of Planar Reinforced Concrete Members Subjected to Fire”, *ACI Structural Journal*, **94** (3), 272-282.
- Huang Z., Burgess I.W. and Plank R.J. (1999a), “Non-linear Analysis of Reinforced Concrete Slabs Subjected to Fire”, *ACI Structural Journal*, **96** (1), 127-135.
- Huang, Z., Burgess, I. W. and Plank R. J. (2003a), “Modelling Membrane Action of Concrete Slabs in Composite Buildings in Fire. Part I: Theoretical Development”, *Journal of Structural Engineering*, ASCE, **129**(8), 1093-1102.
- Huang Z., Burgess I. W. and Plank R. J. (2003b), “A Non-Linear Beam-Column Element for 3D Modelling of General Cross-Sections in Fire”, Research Report, DCSE/03/F/1, Department of Civil & Structural Engineering, The University of Sheffield.
- International Organisation for Standardisation (1985), “ISO 834: Fire Resistance Tests - Elements of Building Construction”.
- Khoury G. A., Grainger B. N. and Sullivan P. J. E. (1985), “Strain of Concrete during First Heating to 600°C under Load”, *Magazine of Concrete Research*, **37**(133), 195-215.
- Lie T.T., and Celikkod B. (1991), “Method to Calculate the Fire Resistance of Circular Reinforced Concrete Columns”, *ACI Material Journal*, **88** (1), 84-91.
- Lin T. D., Ellingwood B. and Piet O. (1987), “Flexural and Shear Behaviour of Reinforced Concrete Beams During Fire Tests”, Report No. NBS-GCR-87-536, Center for Fire Research, National Bureau of Standards.
- Najjar S.R. and Burgess I.W. (1996), “A Non-Linear Analysis for Three-Dimensional Steel Frames in Fire Conditions”, *Engineering Structures*, **18** (1), 77-89.
- Rots J. G., et al (1984), “The Need for Fracture Mechanics Options in Finite Element Models for Concrete Structures, Proc. International Conference on Computer Aided Analysis and Design of Concrete Structures”, F. Damjanic et al, Eds., Pineridge Press, Swansea, Part 1, 19-32.

- Surana K. and Sorem R. (1989), “Geometrically Non-Linear Formulation for Three Dimensional Curved Beam Elements with Large Rotations”, *International Journal for Numerical Methods in Engineering*, **28**, 43-73.
- Terro M. J. (1998), “Numerical Modeling of the Behavior of Concrete Structures in Fire”, *ACI Structural Journal*, 95(2), 183-193.
- Swinden Technology Centre (1999), “The Behaviour of Multi-Storey Steel-Framed Buildings in Fire: A European Joint Research Programme”, British Steel plc, Rotherham, UK.
- Wong S.Y. (2001), “The Structural Response of Industrial Portal Frame Structures in Fire”, PhD Thesis, University of Sheffield.

## Figure Captions

1. Three-dimensional 3-noded beam element configuration.
2. Division of the cross-section of beam-column elements into segments.
3. Concrete tension curve used in the model.
4. Linearly elastic simply supported I-section beam subject to transverse point load at centre.
5. Influence of segmentation within the cross-section of the I-beam on the deflections at mid-span.
6. Influence of different element meshing of the I-beam on the deflections at mid-span.
7. Comparison of predicted and measured temperatures of main reinforcing steel for Columns HH15 and HH17.
8. Comparison of predicted and measured axial displacements for Column HH15.
9. Comparison of predicted and measured axial displacements for Column HH17.
10. Effect of concrete spalling on the behaviour of the Column HH15.
11. Effect of concrete spalling on the behaviour of the Column HH17.
12. Details of tested beams (adapted from Lin *et al.* 1987).
13. Comparison of predicted and measured temperatures of four main reinforcing steel layers for Beam 1.
14. Comparison of predicted and measured temperatures of four main reinforcing steel layers for Beam 5.
15. Comparison of predicted and measured maximum deflections of Beam 1 (ASTM Fire).
16. Comparison of predicted and measured maximum deflections of Beam 3 (ASTM Fire).
17. Comparison of predicted and measured maximum deflections of Beam 5 (SDHI Fire).
18. Comparison of predicted and measured maximum deflections of Beam 6 (SDHI Fire).
19. Influence of concrete spalling on the temperatures of bottom main reinforcing layer for Beam 1.
20. Influence of concrete spalling on maximum deflection for Beam 1.
21. Influence of concrete spalling on maximum deflection for Beam 3.

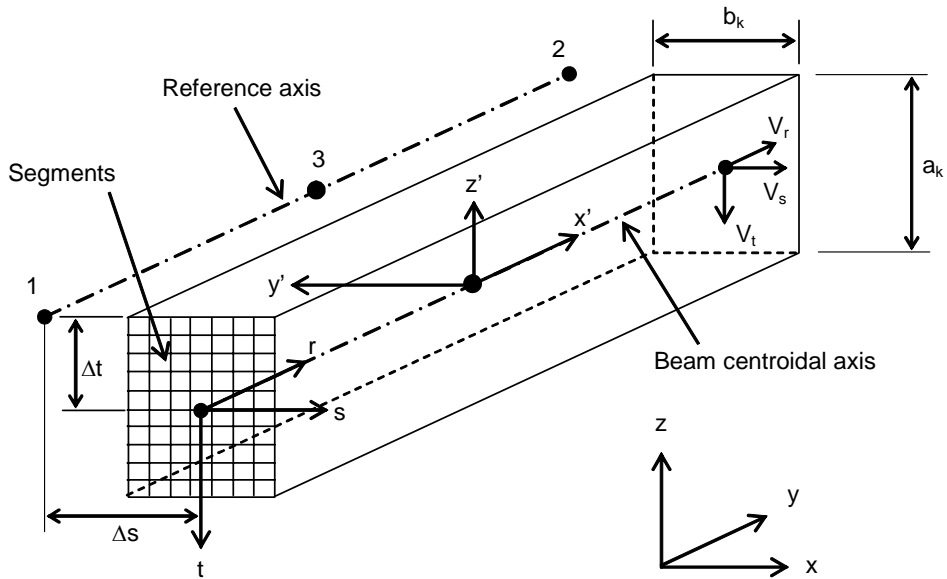


**Fig. 1** Three-dimensional 3-noded beam element configuration.

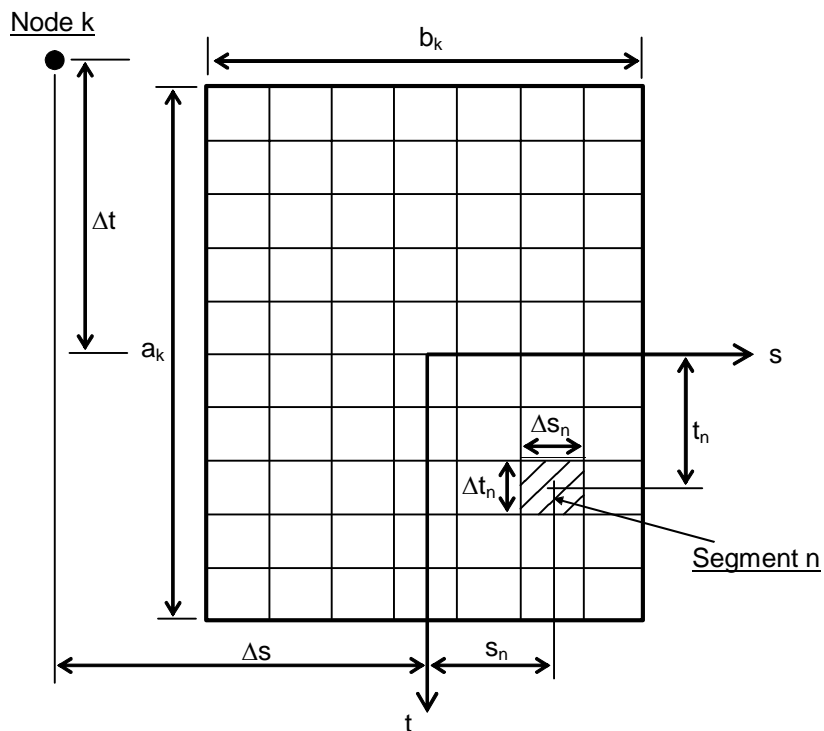


**Fig. 2** Division of the cross-section of beam-column elements into segments.

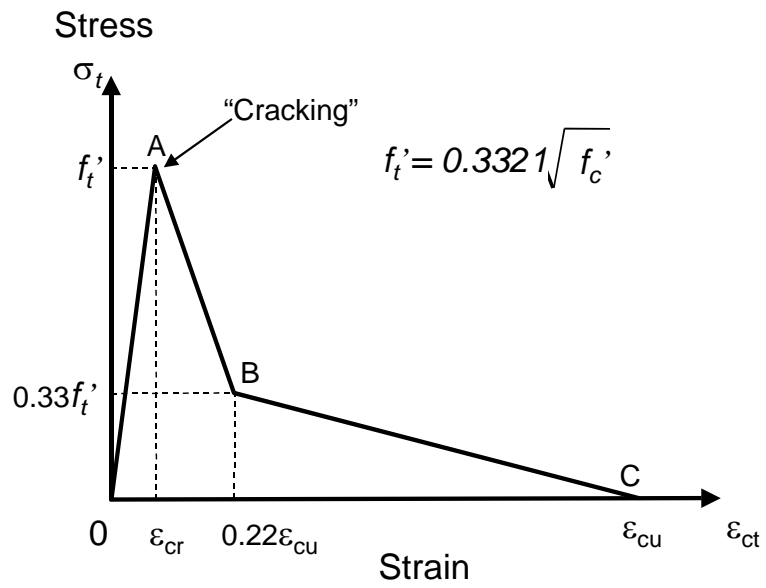


**Fig. 3** Concrete tension curve used in the model.

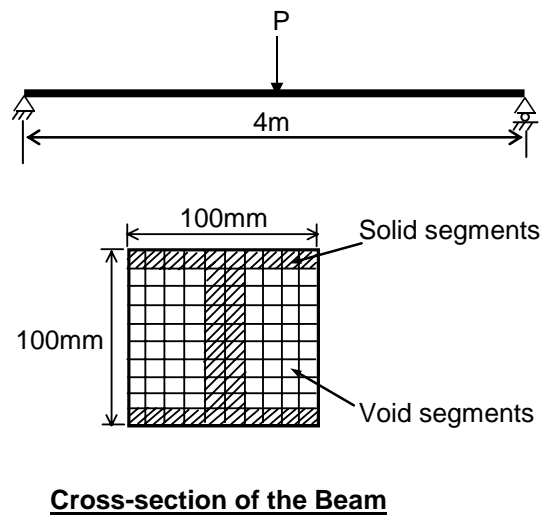


**Fig. 4** Linearly elastic simply supported I-section beam subject to transverse point load at centre.

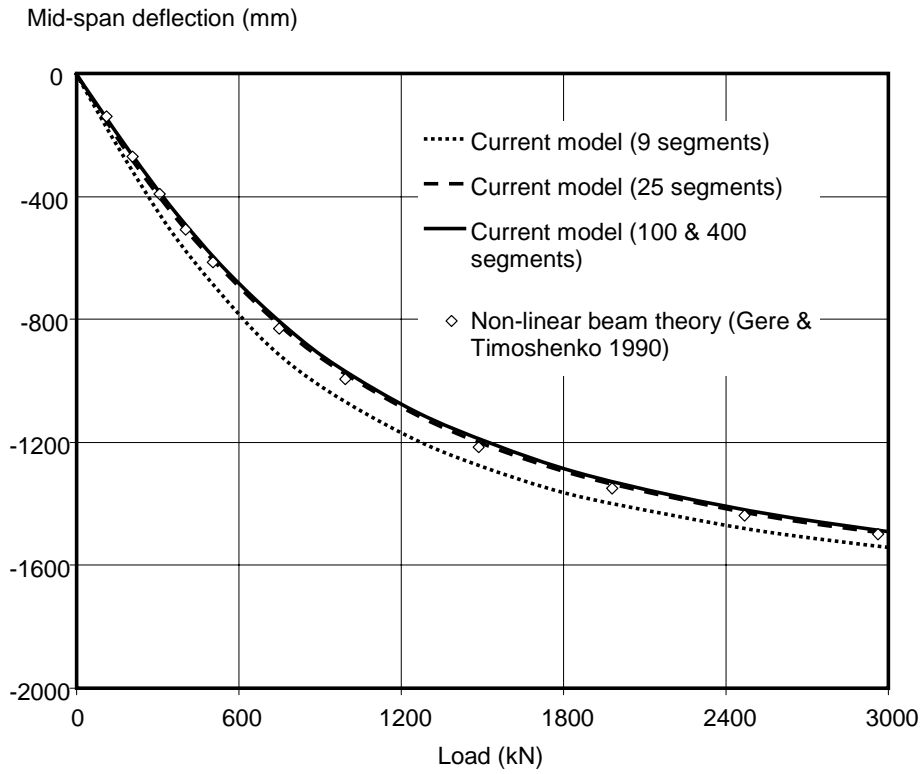


**Fig. 5** Influence of segmentation within the cross-section of the I-beam on the deflections at mid-span.

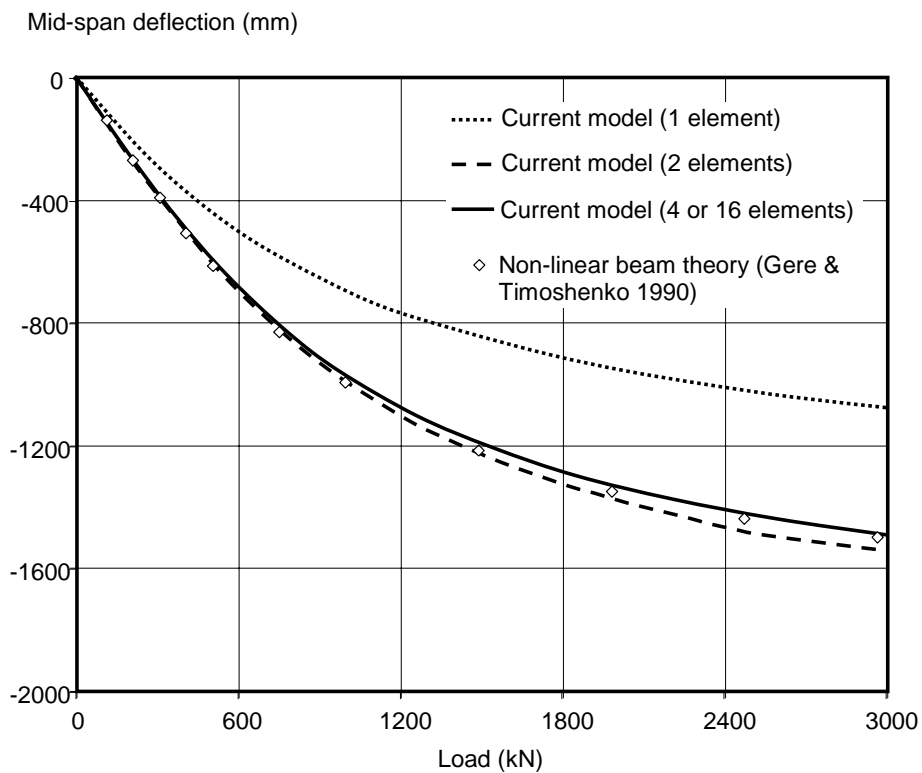


**Fig. 6** Influence of different element meshing of the I-beam on the deflections at mid-span.

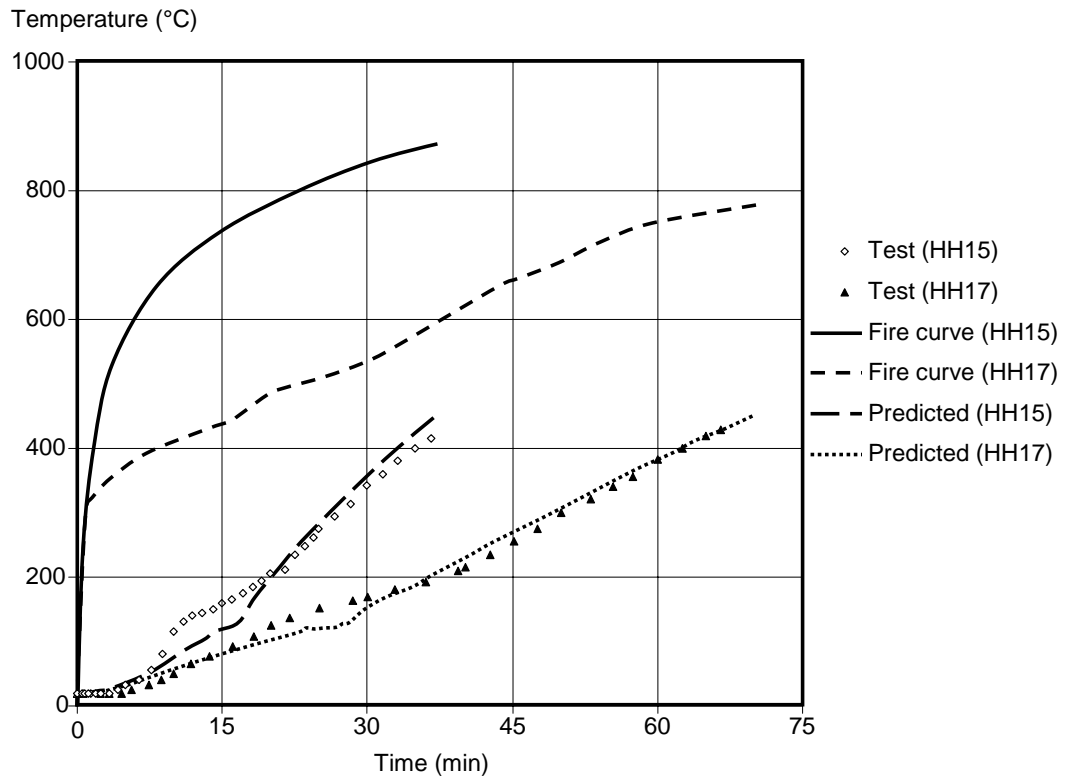


**Fig. 7** Comparison of predicted and measured temperatures of main reinforcing steel for Columns HH15 and HH17.

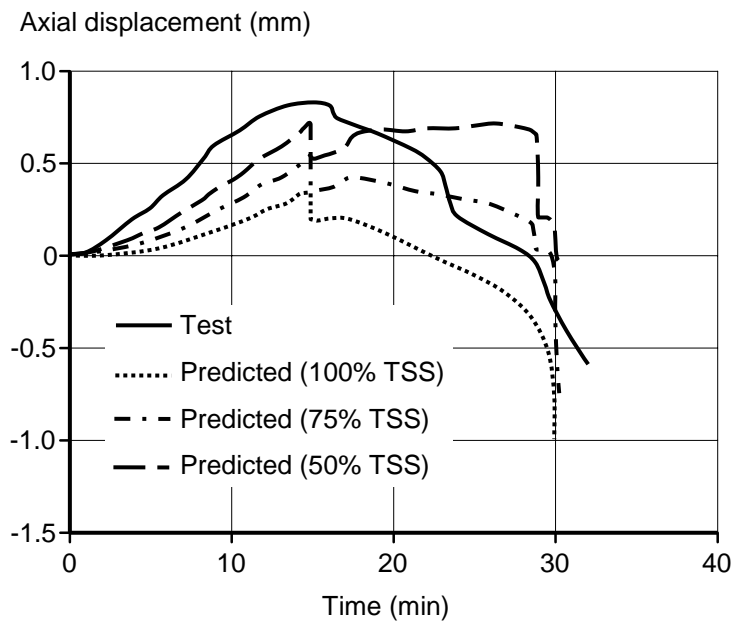


**Fig. 8** Comparison of predicted and measured axial displacements for Column HH15.

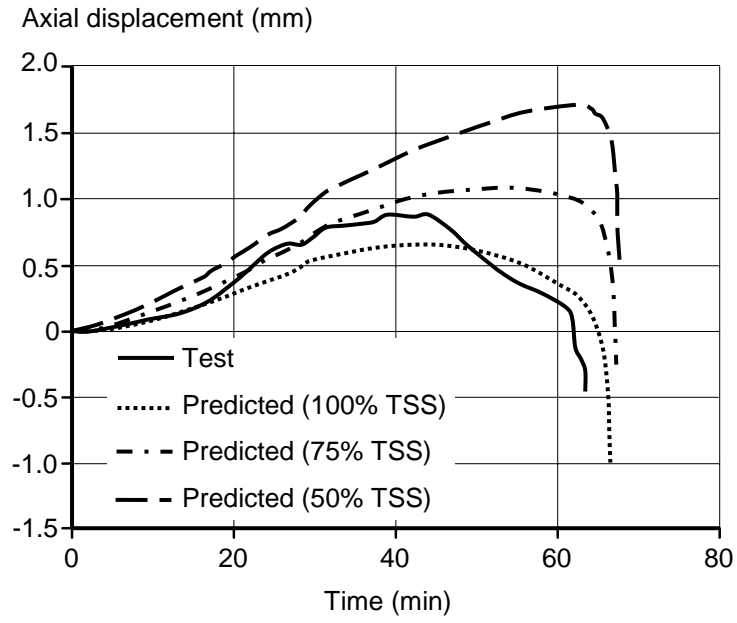


**Fig. 9** Comparison of predicted and measured axial displacements for Column HH17.

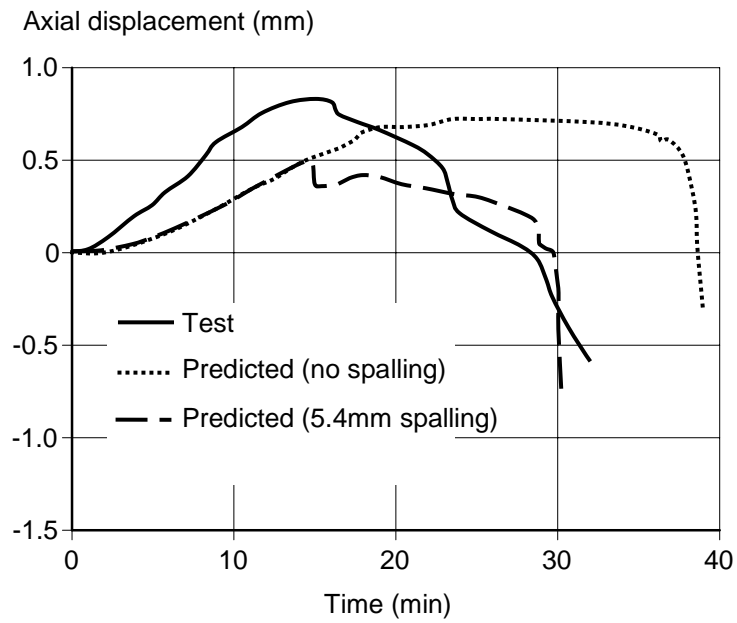


**Fig. 10** Effect of concrete spalling on the behaviour of the Column HH15.

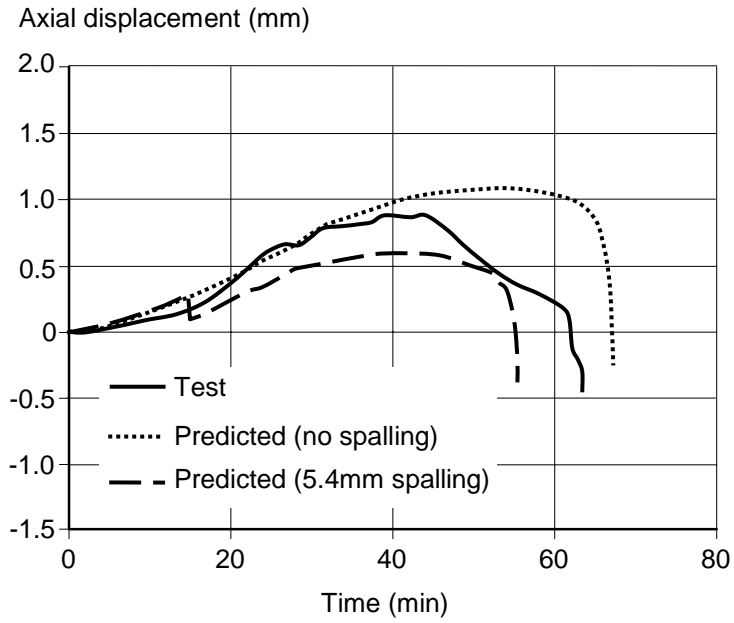


**Fig. 11** Effect of concrete spalling on the behaviour of the Column HH17.

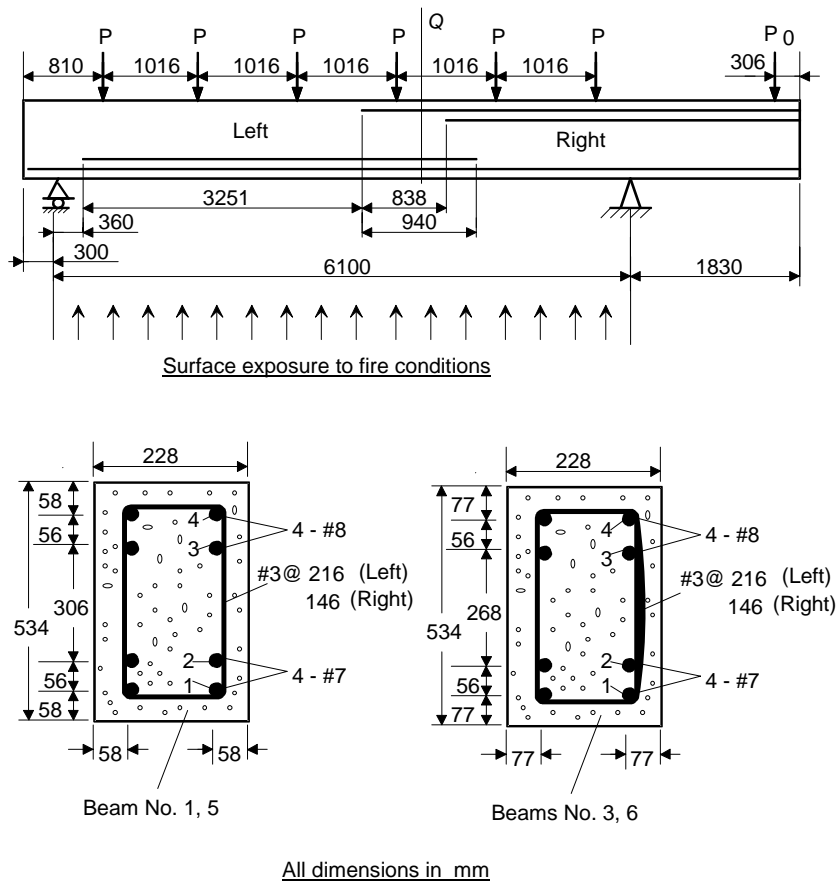


**Fig. 12** Details of tested beams (adapted from Lin *et al.* 1987).

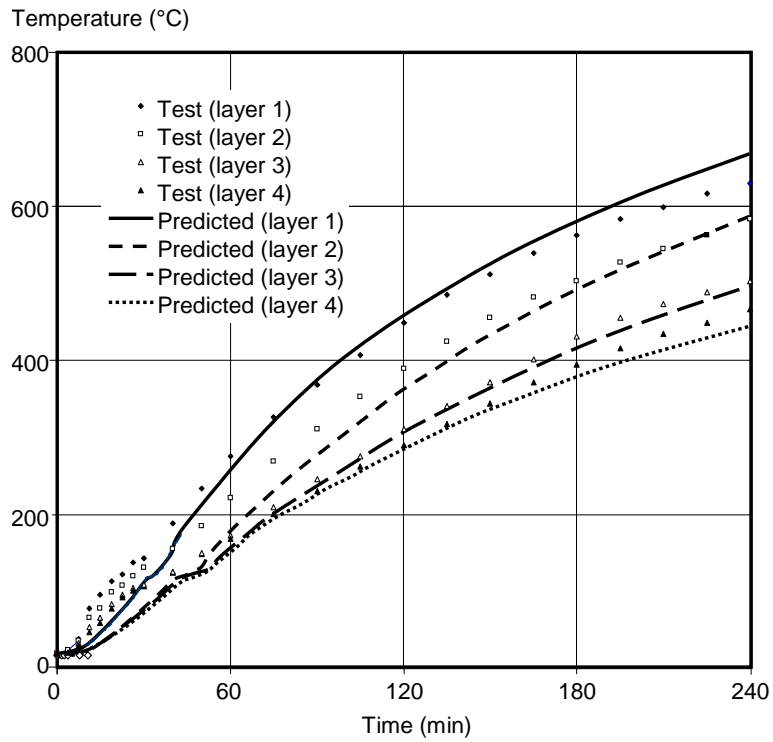


**Fig. 13** Comparison of predicted and measured temperatures of four main reinforcing steel layers for Beam 1.

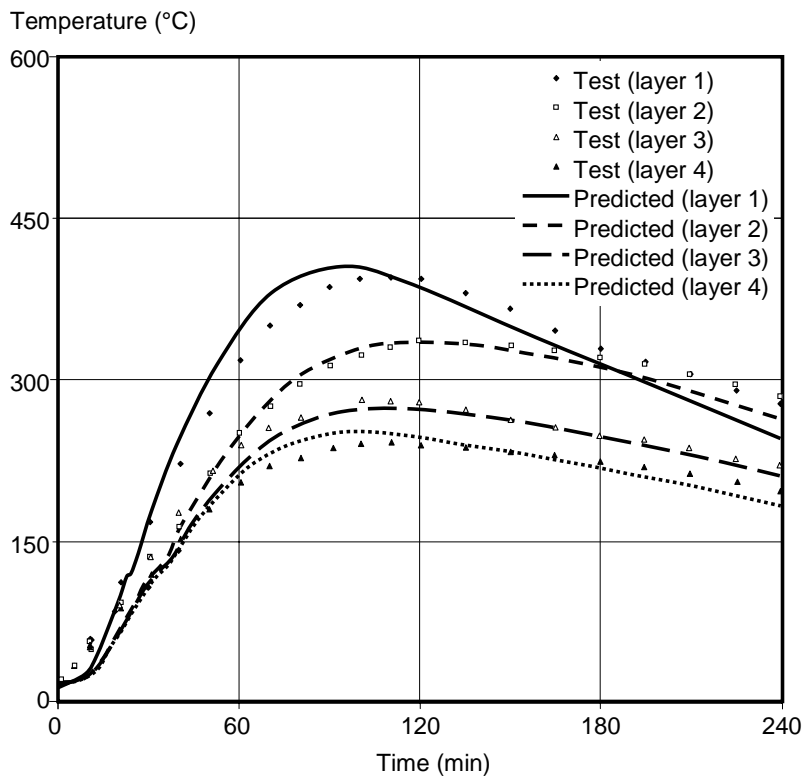


**Fig. 14** Comparison of predicted and measured temperatures of four main reinforcing steel layers for Beam 5.

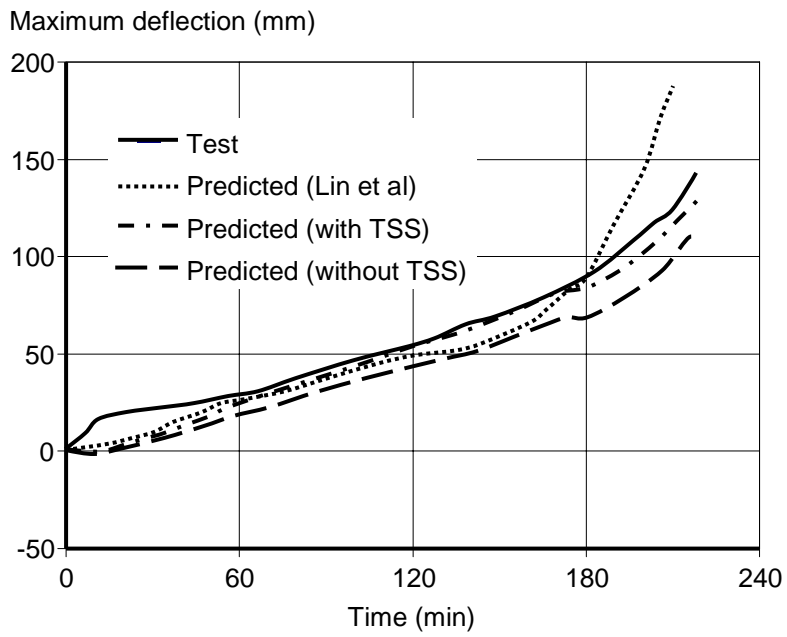


**Fig. 15** Comparison of predicted and measured maximum deflections of Beam 1 (ASTM Fire).

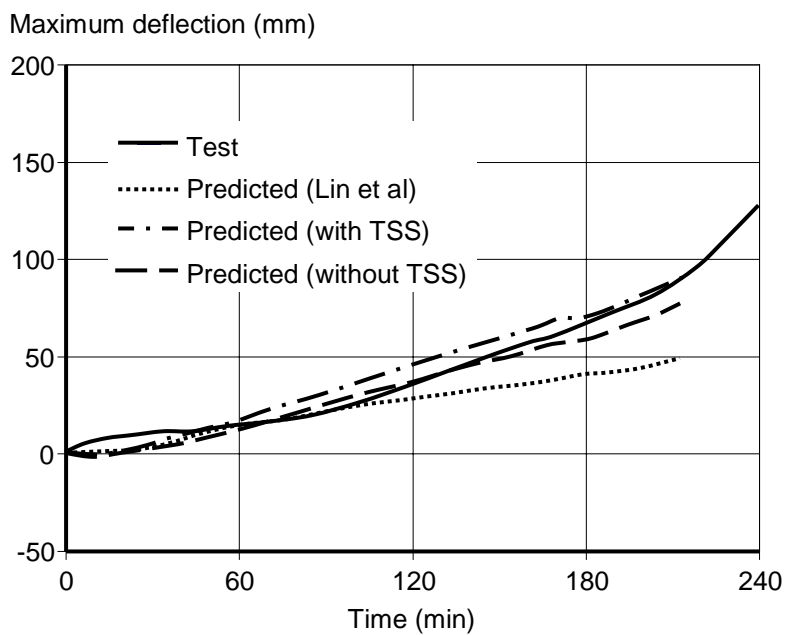


**Fig. 16** Comparison of predicted and measured maximum deflections of Beam 3 (ASTM Fire).

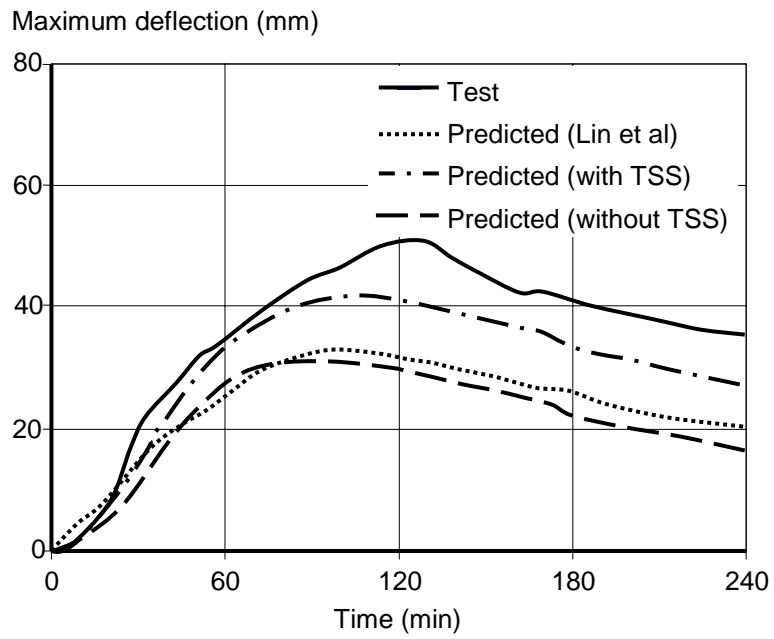


**Fig. 17** \_Comparison of predicted and measured maximum deflections of Beam 5 (SDHI Fire).

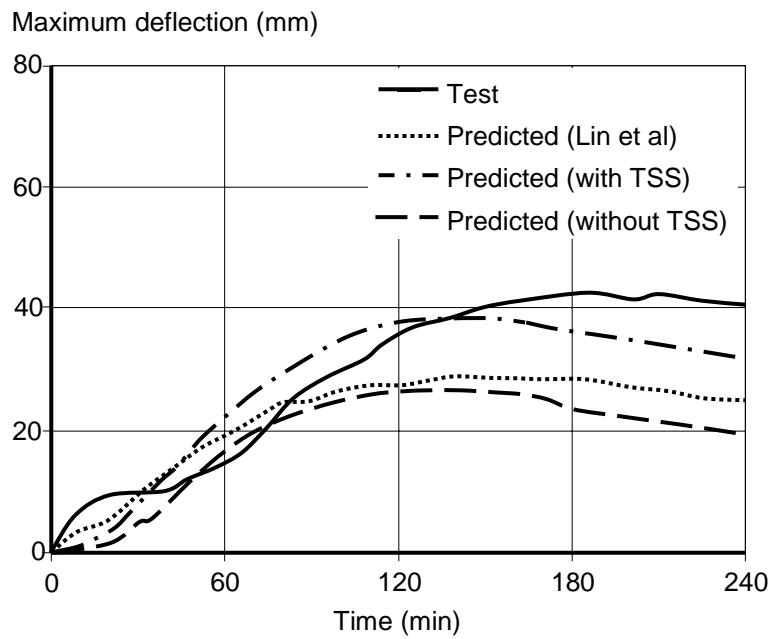


**Fig. 18** Comparison of predicted and measured maximum deflections of Beam 6 (SDHI Fire).

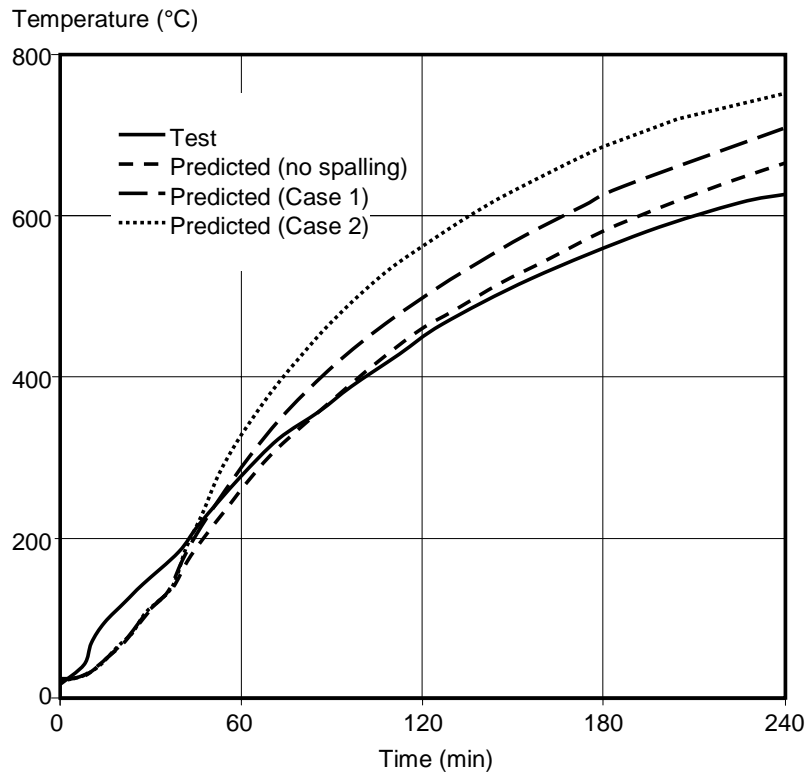


**Fig. 19** Influence of concrete spalling on the temperatures of bottom main reinforcing layer for Beam 1.

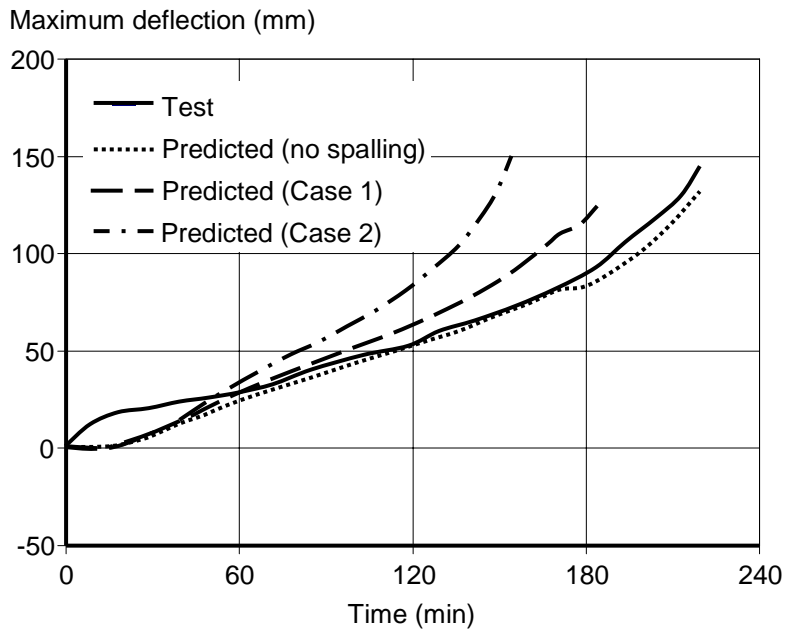


**Fig. 20** Influence of concrete spalling on maximum deflection for Beam 1.

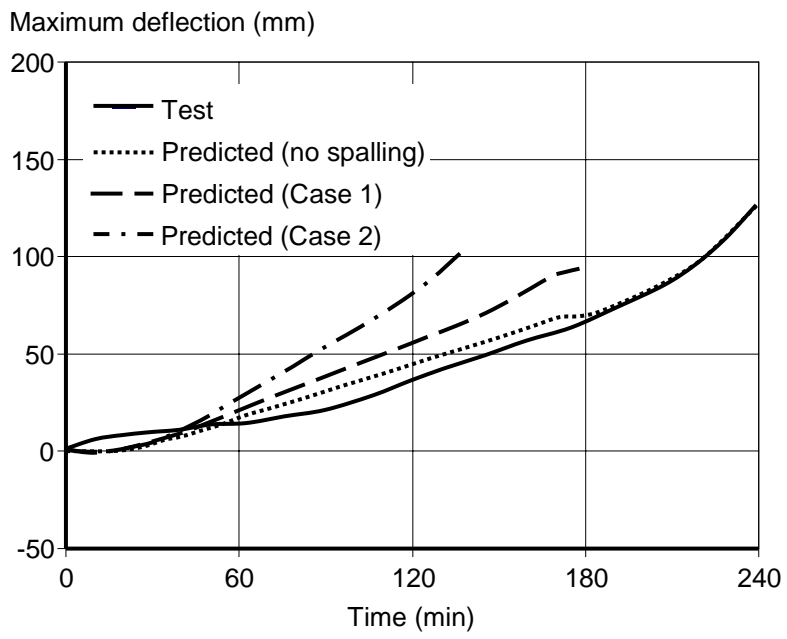


**Fig. 21** Influence of concrete spalling on maximum deflection for Beam 3.